Zhao et al. Nanoscale Research Letters (2017) 12:459
DOI 10.1186/s11671-017-2226-2

Nanoscale Research Letters

NANO EXPRESS Open Access

Facile Synthesis of SiO_2@C Nanoparticles Anchored on MWNT as High-Performance Anode Materials for Li-ion Batteries

Yan Zhao[1], Zhengjun Liu[1], Yongguang Zhang[1*], Almagul Mentbayeva[3], Xin Wang[2], M. Yu. Maximov[4], Baoxi Liu[1], Zhumabay Bakenov[3] and Fuxing Yin[1]

Abstract

Carbon-coated silica nanoparticles anchored on multi-walled carbon nanotubes (SiO_2@C/MWNT composite) were synthesized via a simple and facile sol-gel method followed by heat treatment. Scanning and transmission electron microscopy (SEM and TEM) studies confirmed densely anchoring the carbon-coated SiO_2 nanoparticles onto a flexible MWNT conductive network, which facilitated fast electron and lithium-ion transport and improved structural stability of the composite. As prepared, ternary composite anode showed superior cyclability and rate capability compared to a carbon-coated silica counterpart without MWNT (SiO_2@C). The SiO_2@C/MWNT composite exhibited a high reversible discharge capacity of 744 mAh g^{-1} at the second discharge cycle conducted at a current density of 100 mA g^{-1} as well as an excellent rate capability, delivering a capacity of 475 mAh g^{-1} even at 1000 mA g^{-1}. This enhanced electrochemical performance of SiO_2@C/MWNT ternary composite anode was associated with its unique core-shell and networking structure and a strong mutual synergistic effect among the individual components.

Keywords: Lithium-ion battery, Anode, SiO_2@C/MWNT composite, Sol-gel synthesis

Background

Due to its low lithium intercalation potential as well as excellent cycling performance, graphite has been widely adopted as a commercial anode for lithium-ion batteries (LIBs) [1]. Nevertheless, the theoretical capacity of graphite is only 372 mAh g^{-1}, which cannot fulfill the ever-growing demands for high-performance batteries. Therefore, the development of next-generation anode materials with a larger specific capacity is necessary [2, 3].

Due to a large theoretical capacity of 1965 mAh g^{-1} and a low electrochemical potential, SiO_2 is considered as a potential alternative to traditional carbonaceous anode materials. Furthermore, environmental friendliness, low cost, and natural abundance make SiO_2 a commercial viable electrode material for LIBs. However, its practical application in LIB is commonly hampered by its poor electronic conductivity as well as a drastic volume variation upon charge-discharge process, resulting in particle pulverization and electrode deterioration with cycling [4–6].

One of the effective approaches to overcome these issues is to design SiO_2-based composites by confining SiO_2 particles inside conductive and flexible matrixes [7, 8]. In our previous study, Cu/carbon was introduced into the SiO_2 composite as a dispersive matrix due to its good conductivity and effective buffering of the volume change of SiO_2 [9]. It was shown by Yu et al. [10] that coating the SiO_2 surface with carbon could be an efficient method to enhance its electrochemical performance, because such coating not only improves conductivity of the system but also accommodates the volume changes of the active material upon cycling.

Considering that the contact between SiO_2@C particles is not good enough and the SiO_2@C particles tend to agglomerate during charge/discharge [11] in this work, we report an effective and easy method to synthesize a core-shell SiO_2@C anchored on MWNT via a sol-gel and pyrolysis route. In this composite, a carbon layer is homogeneously coated on the SiO_2 particles, significantly improving the electronic conductivity of the

* Correspondence: yongguangzhang@hebut.edu.cn
[1]School of Materials Science and Engineering, Research Institute for Energy Equipment Materials, Hebei University of Technology, Tianjin 300130, China
Full list of author information is available at the end of the article

system. Furthermore, formation of the 3D electron transportation pathways by a uniform dispersion of MWNT in the composite leads to outstanding electrochemical performance of the composite as an anode material for LIBs.

Methods

Nine cubic centimeter of tetraethyl orthosilicate (TEOS) ($(C_2H_5O)_4Si \geq 99.5\%$) and 9 cm^3 HCl (0.1 mol dm^{-3}) were dispersed in ethanol (16 cm^3) and stirred for 30 min. Meanwhile, 4 g citric acid ($C_6H_8O_7 \cdot H_2O \geq 99.5\%$) and 2.2 cm^3 ethylene glycol ($C_2H_6O_2 \geq 99\%$) were dissolved in deionized water (10 cm^3), and then 1.9 g MWNT dispersion (9 wt%, MWNT aqueous dispersion, Timesnano, Chengdu) (mass ratio of Si and MWNT = 6.6:1) was added into this solution with gentle stirring for 30 min. The two resulting solutions were thoroughly mixed and transferred into an evaporating dish and dried at 55 °C for 10 h. The resulting product was heated under Ar atmosphere for 1 h at 1100 °C to obtain SiO_2@C/MWNT composite. A reference SiO_2@C composite without MWNT was obtained following the same preparation route.

The crystal structure of the samples was characterized by X-ray diffraction (XRD D8 Discover, Bruker) employing Cu Kα radiation. Raman spectra were conducted with Ar-ion laser of 532 nm using the Via Reflex Raman imaging microscope system. The structure and morphology of the SiO_2@C/MWNT composites were studied using scanning electron microscopy (SEM, Hitachi S-4800) and transmission electron microscopy (TEM, JEOL 2100), respectively. Surface elemental analysis was conducted by an energy-dispersive X-ray spectroscopy (EDX) attached to the TEM apparatus. The content of amorphous SiO_2 in SiO_2@C/MWNT composite was estimated by using a thermogravimetric analyzer (STD Q-600) under N_2 flow (30 ml min^{-1}).

The working electrodes were prepared by coating a homogeneous slurry containing 80 wt% active material, 10 wt% acetylene black (MTI, 99.5%), and 10 wt% polyvinylidene fluoride (PVDF) (Kynar, HSV900) binder dissolved in 1-methyl-2-pyrrolidinone (NMP, Sigma-Aldrich, 99.5%) onto a copper current collector by a doctor blade, and further drying at 65 °C for 12 h in a vacuum oven. The resulting SiO_2@C/MWNT and SiO_2@C composite electrode was punched into circular disks with a diameter of 10 mm and a mass loading of ~4 mg cm^{-2}. The coin-type cells with high-purity lithium metal as the counter electrode were assembled in a glove box (MBraun) filled with argon (99.9995%). Galvanostatic charge and discharge tests were conducted on a multichannel battery tester (Neware, BTS-5 V5 mA) with the potential range of 0.01–2.5 V vs. Li/Li^+ at various cycling rates. The Versa STAT electrochemical workstation was used to conduct cyclic voltammetry (CV) tests between 0.01 and 3 V vs. Li/Li^+ at a scanning rate of 0.1 mV s^{-1} and electrochemical impedance spectroscopy (EIS) measurements in a frequency range from 100 kHz to 1 mHz.

Results and Discussion

The phase purity of the SiO_2@C/MWNT ternary composites was confirmed by XRD. It can be seen from Fig. 1 that in contrast with SiO_2@C, the SiO_2@C/MWNT composite shows a typical peak of graphitic carbon at 26.1°, indicating the presence of MWNT with the structure planes (200) [12]. A weak peak around 43° corresponds to a diffusion scattering of amorphous carbon coating, while a broad diffraction peak around 21° is associated with amorphous SiO_2 [13, 14]. All the above results demonstrate that as designed, SiO_2@C/MWNT ternary composite was successfully obtained.

Raman spectroscopy was further performed to investigate the phase compositions in the SiO_2@C/MWNT composite and the SiO_2@C counterpart as shown in Fig. 2. Both samples possess double distinct peaks at 1340 and 1595 cm^{-1}, related to the D and G bands of carbon, respectively [15]. These two vibration peaks demonstrate the low crystallinity of carbon [16]. The D band describes the defect-mediated zone-edge phonons and indicates the disordered carbon, edges, and defects, whereas the G band is a characteristic of the graphitic sheets, which according with the scattering of the E_{2g} mode apperceived for sp^2 domains [17–19]. It is worth to note that the I_D/I_G ratio for SiO_2@C and SiO_2@C/MWNT composites are 0.94 and 0.99, respectively. The I_D/I_G of SiO_2@C/MWNT composites increased compared with that of SiO_2@C as a result of a strong binding interaction and the increased structural defects between Si and O [20, 21].

As displayed in Fig. 3a, SEM confirms the micro/nano structure of SiO_2@C/MWNT composite. The sample shows a disordered configuration with a wide size distribution.

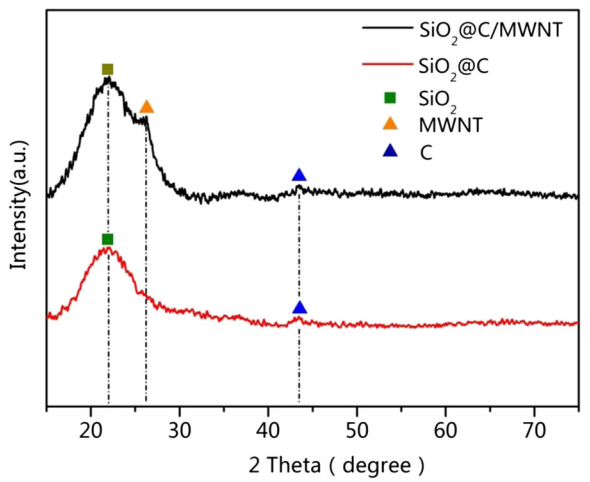

Fig. 1 XRD patterns of SiO_2@C and SiO_2@C/MWNT composites

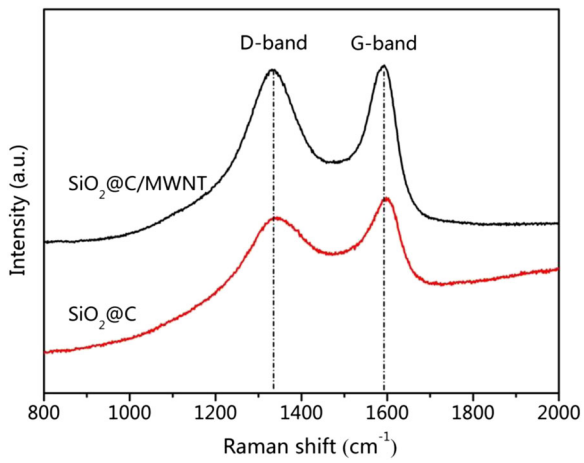

Fig. 2 Raman spectra of SiO_2@C and SiO_2@C/MWNT composites

This could be considered as a verification of the amorphous structure of the material. From the TEM image (Fig. 3b), it can be seen that the MWNT-like bridges are directly connected to the SiO_2@C particles, and this feature could support the structural integrity retention of the composite and favor the fast electron transfer. Meanwhile, MWNT of about 20–50 nm diameter intersperses among SiO_2@C, which has an amorphous structure. The EDX element mapping (Fig. 3 (c1–c4)) indicates that the SiO_2@C/MWNT composite contains homogeneously distributed O, Si, and C. One can see from Fig. 3d that an amorphous carbon layer with a thickness of about 2–7 nm is formed on the surface of SiO_2. A turbostratic structure without crystalline lattice is discovered, indicating that the SiO_2@C/MWNT composite has an amorphous structure. It is worth noting that MWNT is evenly distributed in the disordered matrix. A small amount of a microcrystalline structure domain could be observed in the composite, which lattice fringes with the spacing of about 0.205, 0.215, and 0.411 nm agree well with the spacing between (222), (311), and (111) of SiO_2.

In order to verify the content of amorphous SiO_2 in SiO_2@C/MWNT composite, the TG and DTG data were collected and the results are shown in Fig. 4. The prominent weight loss between 550 and 730 °C, reflected in the TG curve, is related to oxidization of carbon and MWNT. Furthermore, the DTG curve shows two distinct peaks at 635 and 690 °C, which correspond to decomposition reaction of carbon layer and MWNT. Based on the positions of these two curves, the SiO_2 content in the ternary composite can be estimated as ca. 77.5 wt%. Considering these data and the TG results, the mass composition of SiO_2@C/MWNT could be estimated as SiO_2:C :MWNT = 77.5:17: 5.5 wt%.

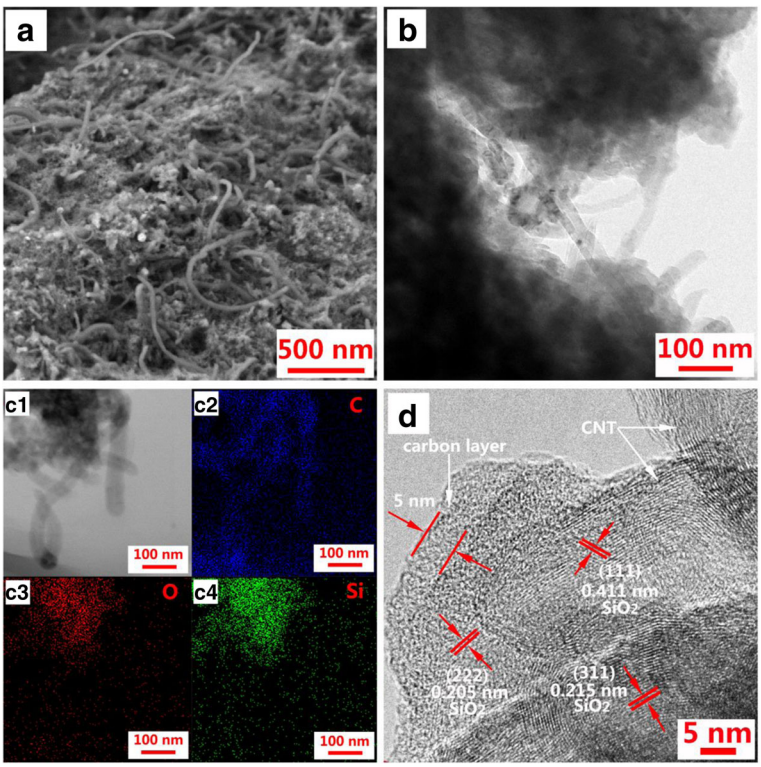

Fig. 3 **a** SEM image and **b** TEM image of SiO_2@C/MWNT composite. **c1** EDX mapping of C (**c2**), O (**c3**), and Si (**c4**) elements. **d** HRTEM image of SiO_2@C/MWNT composite

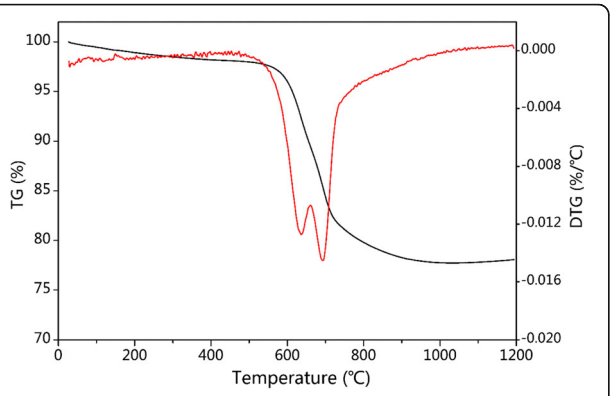

Fig. 4 TG (*black*) and DTG data (*red*) of SiO_2@C/MWNT composite

The CR2025 coin cells were assembled to test the electrochemical performance of the SiO_2@C/MWNT nanocomposite. Figure 5 shows the CV data of SiO_2@C/MWNT. The CV curves present a reduction peak at approximately 0.57 V vs. Li/Li^+ at the first cycle. It is related to the reduction reactions of lithium with SiO_2 resulting in the side products of Li_4SiO_4, $Li_2Si_2O_5$, and Li_2O. Among these, $Li_2Si_2O_5$, as reported, is active in the subsequent cycles, which enhances the electrochemical performance of the system [22], and $Li_2Si_2O_5$ is reversible while the Li_2O and Li_4SiO_4 phases are irreversible upon cycling. The increase of current in the CV curves could be related with this phenomenon. Along with this, this phenomenon could be considered as a part of electrochemical activation of the electrode upon its cycling, which is commonly observed for porous composite systems. A cathodic peak at 0–0.5 V can be observed in the initial cycle, corresponding to the alloying process of SiO_2 [23]. On the other hand, the anodic peak at 0.24–0.9 V is extensive in the Li extraction part, matching well with the de-alloying process between amorphous Li-Si alloys and amorphous SiO_2 [24, 25].

Figure 6a presents the charge/discharge curves of the SiO_2@C/MWNT composite anode. The composite exhibits the initial discharge capacity of about 991 mAh g^{-1} while a corresponding charge capacity is about 615 mAh g^{-1}, and this results in the initial coulombic efficiency of 62%. This relatively low coulombic efficiency could mainly be due to the formation of the solid electrolyte interface (SEI) on the electrode surface during the initial charge/discharge process. The discharge capacity becomes stable after 10 cycles, and the coulombic efficiency increases to ~100%. It is found that the charging potential profile is extraordinarily steep at potentials exceeding 1.4 V, which is due to a glassy state character of SiO_2 with a strong polarization [26]. As shown in Fig. 6b, the potential profiles of the SiO_2@C composite are similar to the profiles of the ternary composite but they exhibit lower capacities.

The counterpart SiO_2@C composite was tested in the same electrochemical environment. As shown in Fig. 7, the comparative cycling performance studies of the binary and ternary electrodes were evaluated at a current

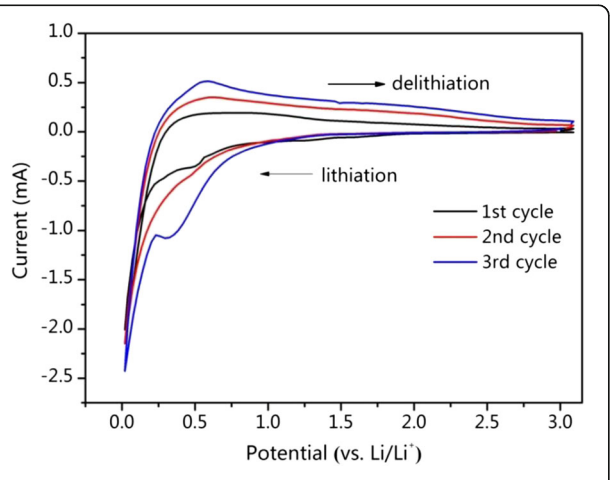

Fig. 5 Cyclic voltammograms of SiO_2@C/MWNT composite electrode at a scan rate of 0.1 mV s^{-1}

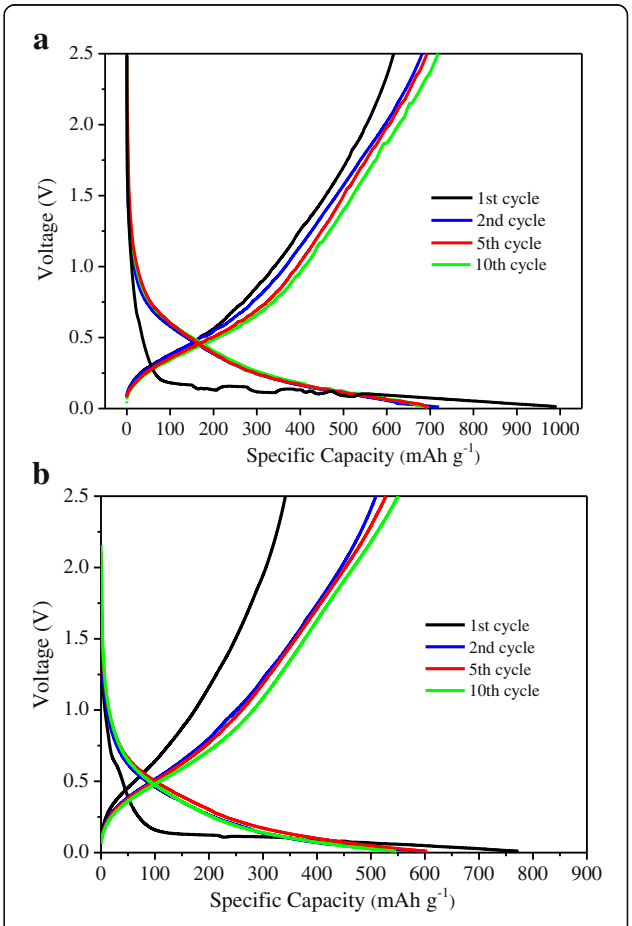

Fig. 6 Charge/discharge profiles of **a** SiO_2@C/MWNT and **b** SiO_2@C composite electrode at a current density of 100 mA g^{-1}

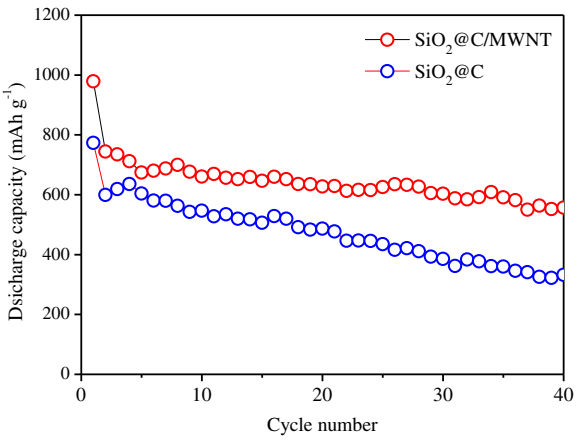

Fig. 7 Cycle performance of SiO_2@C and SiO_2@C/MWNT composite electrodes at a current density of 100 mA g^{-1}

density of 100 mA g^{-1}. It is obvious that the SiO_2@C/MWNT sample shows remarkably enhanced cyclability than its SiO_2@C counterpart. Specifically, the SiO_2@C/MWNT exhibits a high specific capacity of 744 mAh g^{-1} at 100 mA g^{-1} in the second cycle and maintains a capacity of 557 mAh g^{-1} after 40 cycles. However, the corresponding capacity of SiO_2@C retains only a capacity of about 333 mAh g^{-1} at the 40th cycle. The superior cycling stability of the SiO_2@C/MWNT electrode could be attributed to the introduction of well-dispersed MWNT in the composite. Incorporation of MWNT with SiO_2@C is designed to provide pathways for electrolyte/Li^+ ingress and to accommodate the anode active mass volume expansion during cycling [27]. An outstanding rate capability of the SiO_2@C/MWNT ternary electrode is illustrated in Fig. 8. One can see that after 100 cycles, the specific discharge capacity of the cell with the SiO_2@C/MWNT composite cathode slightly decreases, and it exhibits a capacity

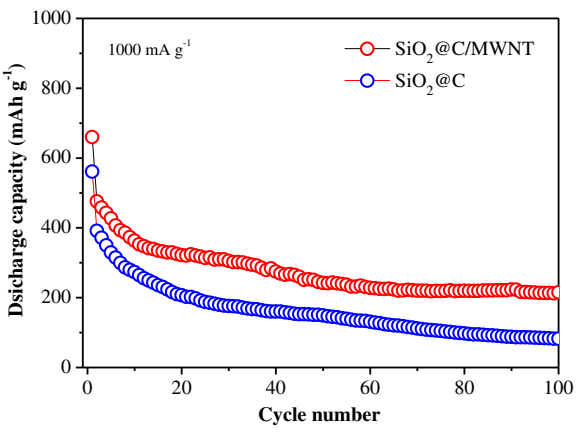

Fig. 8 Rate performance of SiO_2@C and SiO_2@C/MWNT composite electrodes at a current density of 1000 mA g^{-1}

of 215 mAh g^{-1} at a high-current density of 1000 mA g^{-1}, presenting its enhanced electrochemical stability. In the same time, the SiO_2@C composite retains a capacity of only around 95 mAh g^{-1} when cycled at the same current density.

In order to further clarify the role of MWNT networks in the ternary composite, the EIS measurements were performed and the results are shown in Fig. 9. It can be seen that for the fresh cells, the diameter of the compressed semicircle in the high-to-medium frequency range for the SiO_2@C/MWNT ternary electrode corresponds to 95 Ω, which is about half of that for SiO_2@C, indicating that MWNT remarkably improves the conductivity and enhances the charge transfer properties of the ternary electrode. Figure 9b shows changes of EIS upon cycling and an equivalent circuit with a series of constant phase elements (CPE) and resistances obtained from the EIS data fitting. R_E reflect the bulk resistance of the electrolyte. The CPE_1 and R_{SEI} are the charge capacitance and resistance of the solid electrolyte interphase (SEI) layer, respectively. The CPE_2 and R_{CT}

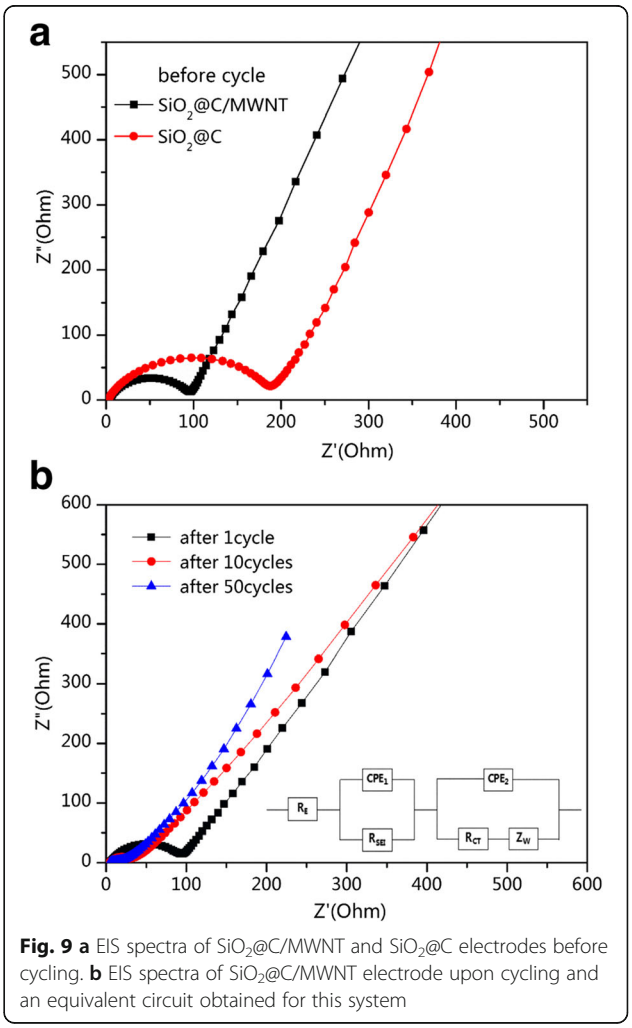

Fig. 9 **a** EIS spectra of SiO_2@C/MWNT and SiO_2@C electrodes before cycling. **b** EIS spectra of SiO_2@C/MWNT electrode upon cycling and an equivalent circuit obtained for this system

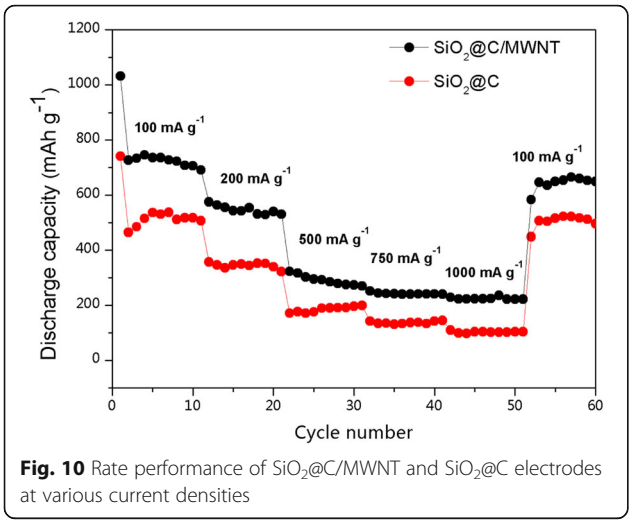

Fig. 10 Rate performance of SiO_2@C/MWNT and SiO_2@C electrodes at various current densities

are related to charge-transfer, which mirrors the lithium ions intercalation into the electrode. The inclined line is generated by the Warburg impedance (Z_W), which represents the lithium-diffusion process within SiO_2@C/MWNT. After the initial cycle, the diameter of the semicircle remains the same at about 95 Ω but the slope of the Warburg component decreases compared with that of a fresh cell, reflecting the lithium-ion diffusion process within the electrode. Further, the resistance of the ternary electrode decreases to about 30 Ω due to the activation process. After 50 cycles, the diameter of the semicircle tends to stabilize, i.e., there is no remarkable impedance change, which evidences the stability of the ternary electrode upon cycling and its ability to be well adapted to the volume changes. These results confirm that MWNT can obviously improve the conductivity and enhance the structure stability of the SiO_2@C/MWNT ternary electrode.

Furthermore the SiO_2@C/MWNT nanocomposite electrode exhibits a good-rate capability as shown in Fig. 10. The SiO_2@C/MWNT electrode delivers reversible capacities of ~710, 570, 300, 250, and 220 mAh g^{-1} at current densities of 100, 200, 500, 750 and 1000 mA g^{-1}, respectively. When further, the current density was returned to 100 mA g^{-1}, about 95% of the initial capacity could be recovered, indicating a good structural and electrochemical stability of the system. It can also be seen from Fig. 10 that the reversible capacities of SiO_2@C are lower than that of SiO_2@C/MWNT over a whole range of the current densities studied. It can be concluded that the MWNT component enhances the conditions for lithium-ion diffusion and the electric conductivity of the composite, favoring its rate capability.

Table 1 compares the performance data reported for the silicon anode for lithium-ion batteries with the results of this work. It can be seen that the SiO_2@C/MWNT electrode prepared in this work exhibits an enhanced electrochemical performance compared with those reported previously. One can see that the reversible capacity and capacity retention of SiO_2@C/MWNT at 40th cycles are higher than for most of other silicon electrodes reported in the literature. These results indicate that the SiO_2@C/MWNT composite with a carbon containing layer structure and MWNT could be considered as a promising anode for high-performance Li-ion batteries.

Table 1 Performance comparison of SiO_2 and SiO_2@C electrodes for LIBs

Materials	Reversible capacity (mAh g^{-1})	Initial discharge/charge specific capacity (mAh g^{-1})	Current density	Cutoff potential range (*V*)	Ref.
Carbon-coated SiO_2 nanoparticles	Above 500 (50th)	900/536	50 mA g^{-1}	0.001–3	[10]
Silicon oxide-carbon	601 (100th)	1055/458	70 mA g^{-1}	0.01–2	[28]
SiO_2@GA composite	300 (110th)	1042.7/453.3	500 mA g^{-1}	0.01–3	[29]
SiOx@C	630 (150th)	1160/820	50 mA g^{-1}	0.01–3	[22]
Ag-deposited 3D porous Si	755 (50th)	1906/–	50 mA g^{-1}	0.02–1.5	[30]
SiO_2@C/MWNT	557 (40th)	991/615	100 mA g^{-1}	0.01–2.5	This work

Conclusions

The SiO_2@C/MWNT ternary composite was successfully synthesized by a simple sol-gel method using low-cost citric acid and TEOS as starting materials, followed by heat treatment. Due to its unique core-shell and network structure and enhanced contact between its individual components, the resulting ternary composite cathode exhibited a remarkably enhanced electrochemical performance compared with the binary SiO_2@C counterpart. Considering the simplicity and efficiency of the preparation process and outstanding electrochemical performance, the SiO_2@C/MWNT composite can be considered as a promising anode material for the next generation lithium-ion batteries.

Abbreviations

CV: Cyclic voltammetry; EDX: Energy-dispersive X-ray spectroscopy; LIBs: Lithium-ion batteries; MWNT: Multi-walled carbon nanotube; SEM: Scanning electron microscope; SiO_2: Silica; SiO_2@C: Carbon-coated silica composite; SiO_2@C/MWNT: SiO_2@C nanoparticles anchored on MWNT; TEM: Transmission electron microscope; TEOS: Tetraethyl orthosilicate; XRD: X-ray diffraction

Acknowledgements

The authors acknowledge the financial support from the National Natural Science Foundation of China (Grant No. 21406052), the Program for the

Outstanding Young Talents of Hebei Province (Grant No. BJ2014010), Scientific Research Foundation for Selected Overseas Chinese Scholars, Ministry of Human Resources and Social Security of China (Grant No. CG2015003002), and the targeted program 0143/PCF-14 «Fundamental bases of the processes, based on electrochemical formations» from the Ministry of Education and Science of the Republic of Kazakhstan.

Authors' Contributions

YZ and YGZ conceived and designed the experiments. YZ and ZL carried out the experiments. ZL, AM, XW, and MYM analyzed the data. AM, BL, FY, and ZB contributed in the drafting and revision of the manuscript. YGZ supervised the work and finalized the manuscript. All authors read and approved the final manuscript.

Competing Interests

The authors declare that they have no competing interests.

Publisher's Note

Author details

[1]School of Materials Science and Engineering, Research Institute for Energy Equipment Materials, Hebei University of Technology, Tianjin 300130, China. [2]Synergy Innovation Institute of GDUT, Heyuan, Guangdong Province, China. [3]Institute of Batteries LLC, National Laboratory Astana, School of Engineering, Nazarbayev University, 53 Kabanbay Batyr Avenue, Astana 010000, Kazakhstan. [4]Peter the Great Saint-Petersburg Polytechnic University, Saint Petersburg 195221, Russia.

Received: 8 February 2017 Accepted: 9 July 2017
Published online: 18 July 2017

References

1. Kim H, Lee EJ, Sun YK (2014) Recent advances in the Si-based nanocomposite materials as high capacity anode materials for lithium ion batteries. Mater Today 17:285–297
2. Zhang YG, Li Y, Li HP, Zhao Y, Yin F, Bakenov Z (2016) Electrochemical performance of carbon-encapsulated Fe_3O_4 nanoparticles in lithium-ion batteries: morphology and particle size effects. Electrochim Acta 216:475–483
3. Li HP, Wei YQ, Zhang YG, Zhang C, Wang G, Zhao Y et al (2016) In situ sol-gel synthesis of ultrafine ZnO nanocrystals anchored on graphene as anode material for lithium-ion batteries. Ceram Int 42:12371–12377
4. Chakraborty J, Please CP, Goriely A, Chapman SJ (2014) Combining mechanical and chemical effects in the deformation and failure of a cylindrical electrode particle in a Li-ion battery. Int J Solids Struct 54:66–81
5. Mooney JJ, Witt CJ, Mohr MT. Method and system for determining the depth of an electrically conductive body in a medium having a known conductivity and a known permeability by measuring phase difference between a primary and secondary magnetic field. US; 1992.
6. Zhang YG, Zhao Y, Konarov A, Gosselink D, Li Z, Chen P (2013) One-pot approach to synthesize PPy@S core-shell nanocomposite cathode for Li/S batteries. J Nanopart Res 15:2007
7. Yin D, Zhang Q, Zhang H, Yin C (2010) Fabrication of covalently-bonded polystyrene/SiO_2 composites by Pickering emulsion polymerization. J Polym Res 17:689–696
8. Wang R, Wang X, Xi X, Hu R, Jiang J (2012) Preparation and photocatalytic activity of magnetic Fe_3O_4/SiO_2/TiO_2 composites. Adv Mater Sci Eng 2012: 409379
9. Li M, Li J, Li K, Zhao Y, Zhang Y, Gosselink D et al (2013) SiO_2/Cu/polyacrylonitrile-C composite as anode material in lithium ion batteries. J Power Sources 240:659–666
10. Yao Y, Zhang J, Xue L, Huang T, Yu A (2011) Carbon-coated SiO_2 nanoparticles as anode material for lithium ion batteries. J Power Sources 196:10240–10243
11. Ren Y, Wu X, Li M (2016) Highly stable SiO_x/multiwall carbon nanotube/N-doped carbon composite as anodes for lithium-ion batteries. Electrochim Acta 206:328–336
12. Dong Y, Md K, Chui YS, Xia Y, Cao C, Lee JM et al (2015) Synthesis of CNT@Fe_3O_4-C hybrid nanocables as anode materials with enhanced electrochemical performance for lithium ion batteries. Electrochim Acta 176: 1332–1337
13. Wang J, Zhao H, He J, Wang C, Wang J (2011) Nano-sized SiO_x/C composite anode for lithium ion batteries. J Power Sources 196:4811–4815
14. Godoy NV, Segatelli MG (2015) Kinetic investigation of thermal formation processes of SiOC glasses derived from C-containing hybrid polymeric networks. J Braz Chem Soc 26:899–909
15. Muraliganth T, Murugan AV, Manthiram A (2009) Facile synthesis of carbon-decorated single-crystalline Fe_3O_4nanowires and their application as high performance anode in lithium ion batteries. Chem Commun 41:7360–7362
16. Park JM, Kim DS (2000) The influence of crystallinity on interfacial properties of carbon and SiC two-fiber/polyetheretherketone (PEEK) composites. Polym Compos 21:789–797
17. Zhou X, Yin YX, Wan LJ, Guo YG (2012) Self-assembled nanocomposite of silicon nanoparticles encapsulated in graphene through electrostatic attraction for lithium-ion batteries. Adv Energy Mater 2:1086–1090
18. Chen S, Yeoh W, Liu Q, Wang G (2012) Chemical-free synthesis of grapheme-carbon nanotube hybrid materials for reversible lithium storage in lithium-ion batteries. Carbon 50:4557–4565
19. Xiao L, Wu D, Han S, Huang Y, Li S, He M et al (2013) Self-assembled Fe_2O_3/graphene aerogel with high lithium storage performance. ACS Appl Mater Interfaces 5:3764–3769
20. Liu Y, Ying Y, Mao Y, Gu L, Wang Y, Peng X (2013) CuO nanosheets/rGO hybrid lamellar films with enhanced capacitance. Nanoscale 5:9134–9140
21. Liu J, Feng H, Wang X, Qian D, Jiang J, Li J et al (2014) Self-assembly of nano/micro-structured Fe_3O_4 microspheres among 3D rGO/CNTs hierarchical networks with superior lithium storage performances. Nanotechnology 25:225401
22. Li M, Zeng Y, Ren Y, Zeng C, Gu J, Feng X et al (2015) Fabrication and lithium storage performance of sugar apple-shaped SiO_x@C nanocomposite spheres. J Power Sources 288:53–61
23. Tang YY, Xia XH, Yu YX, Shi SJ, Chen J, Zhang YQ et al (2013) Cobalt nanomountain array supported silicon film anode for high-performance lithium ion batteries. Electrochim Acta 88:664–670
24. Pereira-Nabais C, Światowska J, Chagnes A, Ozanam F, Gohier A, Tran-Van P et al (2013) Interphase chemistry of Si electrodes used as anodes in Li-ion batteries. Appl Surf Sci 266:5–16
25. Hatchard TD, Dahn JR (2004) In situ XRD and electrochemical study of the reaction of lithium with amorphous silicon. J Electrochem Soc 151:838–842
26. Guo H, Mao R, Yang X, Chen J (2012) Hollow nanotubular SiOx templated by cellulose fibers for lithium ion batteries. Electrochim Acta 74:271–274
27. Zhang YG, Wei YQ, Li HP, Zhao Y, Yin F, Wang X (2016) Simple fabrication of free-standing ZnO/graphene/carbon nanotube composite anode for lithium-ion batteries. Mater Lett 184:235–238
28. Kim JY, Nguyen DT, Kang JS, Song SW (2015) Facile synthesis and stable cycling ability of hollow submicron silicon oxide-carbon composite anode material for Li-ion battery. J Alloys Compd 633:92–96
29. Meng JK, Cao Y, Suo Y, Liu YS, Zhang JM, Zheng XC (2015) Facile fabrication of 3D SiO2@Graphene aerogel composites as anode material for lithium ion batteries. Electrochim Acta 176:1001–1009
30. Wang QT, Han LJ, Zhang X, Li J, Zhou XZ, Lei ZQ (2016) Ag-deposited 3D porous Si anodes with enhanced cycling stability for lithium-ion batteries. Mater Lett 185:558–560